JOURNAL OF GUIDANCE, CONTROL, AND DYNAMICS
Vol. 20, No. 2, March–April 1997

Robustness of a Variable Structure Control System for Maneuverable Flight Vehicles

Mario Innocenti*
University of Pisa, 56126 Pisa, Italy
and
Ajay Thukral†
Tuskegee University, Alabama 36088

One of the key issues related to design of supermaneuverable missiles is precise control during rapid maneuvers. An autopilot synthesis for a marginally stable air-to-air missile with the inclusion of on/off reaction jets to supplement pitch control provided by the elevators is presented. The proposed control method is an extension of variable structure control theory to include simultaneous use of continuous and discontinuous actuators. Stability and robustness issues are addressed, and autopilot synthesis is then carried out. A blending of aerodynamic and propulsive controls is also introduced, based on linear programming that optimizes continuous and discontinuous control, into a single input at low angles of attack. Results from digital simulation of a controlled 180-deg maneuver of a hypothetical next-generation air-to-air missile model show that the proposed method provides stable and robust control over a wide range of flight conditions.

Nomenclature

A, B, A_m, B_m	= system matrices for the missile and model, respectively
L, D, M	= lift, drag, pitching moment
m, I_y	= mass, pitching moment of inertia
$s(), c()$	= sin( ), cos( )
T_E, T_{RCS}	= main engine thrust and reaction jet thrust setting
u, w, q	= body axes velocity components and pitch rate
$\boldsymbol{x}, \boldsymbol{u}$	= state vector, control vector
$\boldsymbol{x}_m, \boldsymbol{u}_m$	= state vector, commanded input vector for model
α, α_c	= angle of attack, critical angle of attack
Γ, Θ	= flight-path and attitude angles
Δ	= elevator deflection (also, equivalent control input), reaction jet switch $[-1, 0, +1]$
θ, γ	= perturbed attitude and flight path angles

I. Introduction

CONSIDERABLE work is currently being done in the area of flight vehicle maneuverability enhancement through the extension of the angle-of-attack envelope. In the fixed wing community, basic research and in-flight experimentation has been carried out to explore the advantages of poststall controlled flight, in the general framework of agility.[1–4] Although the agility aspects lend themselves to include a variety of system's components as part of a general mission effectiveness improvement, the dynamics and control challenges focus mainly on two areas: 1) the use of alternate actuation schemes to complement and/or replace aerodynamic control and 2) the development of basic control methodologies. The central issue to the former aspect is to provide attitude control at angles of attack in excess of 30–50 deg (i.e., beyond the critical angle-of-attack α_c) during which the elevator looses its control effectiveness. Such large angles of attack are expected in rapid maneuvers. For these systems, the second aspect of robust design becomes essential, because the system to be controlled has not only poorly known aerodynamic characteristics but also rapidly changing parameters, nonlinearities in inertia and aerodynamic forces, dynamic and aerodynamic coupling among the various degrees of freedom, and the presence of uncertainties. In this respect, research activities must address the needs of control design of uncertain nonlinear systems and the selection of alternate actuation procedures to supplement and enhance the effectiveness of conventional aerodynamic control surfaces to maintain controllability, maneuverability, and tracking, when aerodynamic control is lost. This last aspect is addressed typically by altering the fluid flow around the body in an active fashion and by introducing independent control capabilities via propulsive effectors. Propulsive control comes usually in the form of thrust diverters or thrust vectoring control and/or localized discontinuous moment generation by using auxiliary thrusters or reaction jet control.[4–7] From a control theoretic standpoint, the methodologies may differ depending on the system's nonlinear behavior being confined mainly to the plant itself (vehicle and thrust vector control) or being an integral part of the control system implementation [vehicle and reaction jet control (RJC)] as well. Feedback linearization, dynamic inversion, and point-linearization design with gain scheduling appear more consistent with the continuous control action provided by thrust vectoring and aerodynamics. The use of on/off reaction jets, on the other hand, suggests direct nonlinear approaches, such as relay-based control, bang-bang, and variable structure techniques, successfully applied over the years in the area of electric drives.

The present paper stems from the preliminary work presented in Refs. 8 and 9. The paper is structured as follows. Section II describes the mission scenario, briefly reviews the model dynamics, formulates the autopilot structure, and optimizes blending between actuators by using a linear programming approach.[10] Section III presents the stability and robustness analysis for systems using a combination of continuous (aerodynamic) controller and discontinuous (on/off reaction jets) controllers. The analytical results are supported by nonlinear simulation. Finally, Sec. IV presents the conclusions and comments.

II. Autopilot Structure

This section reviews the mission scenario, the dynamic properties of the controlled plant, and the controller structure and discusses the performance improvement of the autopilot under nominal flight conditions.[9,11]

A. Mission Scenario

The plant to be controlled is representative of a generic air-to-air missile, whose mission objective is to perform a fast heading reversal maneuver in the vertical plane with no constraints on the angle of attack. The flight-path reversal maneuver selected includes both the stalled and unstalled phases of flight. For the purpose of control,

Received June 26, 1995; revision received Oct. 18, 1996; accepted for publication Dec. 6, 1996.

*Associate Professor, Department of Electrical Systems and Automation. Associate Fellow AIAA.
†Assistant Professor, Department of Mechanical Engineering.

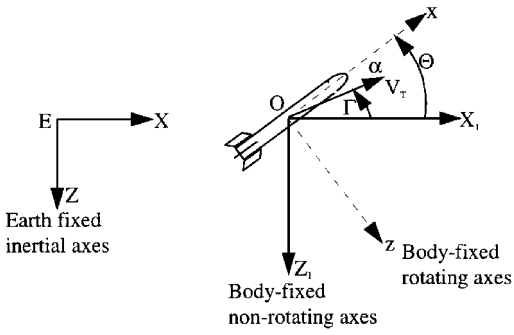

Fig. 1 Missile configuration and references.

the maneuver is broken down into three phases: phase I corresponds to the onset of the maneuver and ends when the missile reaches α_c, phase II is a short duration phase during which the missile is stalled ($\alpha > \alpha_c$) and is rapidly pitching about its y axis toward the commanded final attitude, and phase III is the final steady-state acquisition where flight is performed at low angle of attack ($\alpha < \alpha_c$).

B. Missile Dynamics

The detailed derivation[6,9,11] of the governing nonlinear equations of motion in the vertical plane and the actuator dynamics is straightforward and is not presented here. The aerodynamic model used can be considered as a first approximation and is based on a combination of DATCOM[12] calculations for the unstalled phase flight and analytical predictions during the stalled phase of flight,[13] due to the absence of more accurate data. In summary, using the standard body axes notation,[9,11] as shown in Fig. 1, we can write

$$m\begin{bmatrix}\dot{u}+qw\\ \dot{w}-qu\end{bmatrix}=\begin{bmatrix}c\Theta & -s\Theta\\ s\Theta & c\Theta\end{bmatrix}\times\begin{bmatrix}-Dc\Gamma-Ls\Gamma+T_Ec\Theta-T_{RCS}s\Theta U_T\\ Ds\Gamma-Lc\Gamma-T_Es\Theta-T_{RCS}c\Theta U_T+mg\end{bmatrix} \tag{1}$$

$$I_y\dot{q}=M \qquad \Gamma=\Theta-\alpha \tag{2}$$

The model described by Eqs. (1) and (2) gives the inertial-based nonlinear equations used for nonlinear simulation purposes where lift, drag, and pitching moment are functions of angle of attack and Mach number. For the autopilot design, linearized plant models are obtained from Eqs. (1) and (2). The linearized model is basically the short-period approximation and is used for autopilot design purposes. Two linearized plant models, one for the high-angle-of-attack regime and the other for low-angle-of-attack regime, were obtained corresponding to stalled and unstalled states of flight because they exhibit very distinct dynamic response. From Eqs. (1) and (2) and using short-period approximations about trim values $(\boldsymbol{x}_0, \boldsymbol{u}_0)$, the linearized equations of motion for the entire maneuver in the functional form can be written as

$$\dot{\boldsymbol{x}}(\alpha,t)=A(\alpha)\boldsymbol{x}(\alpha,t)+B(\alpha)\boldsymbol{u}(\alpha,t)+\boldsymbol{d}(\alpha)+\boldsymbol{f}(\alpha,\boldsymbol{x}_0,\boldsymbol{u}_0) \tag{3}$$

The functional dependence of Eq. (3) on the angle of attack simply indicates the two different models corresponding to the missile below stall ($\alpha < \alpha_c$) or beyond it ($\alpha > \alpha_c$) in a single equation. Thus, for $\alpha < \alpha_c$,

$$\boldsymbol{x}=[\Theta \quad q \quad \Gamma]^T, \qquad \boldsymbol{u}=[\Delta \quad U_T]^T$$

$$\boldsymbol{x}_0=[\theta_0 \quad 0 \quad \gamma_0]^T, \qquad \boldsymbol{u}_0=0, \qquad \boldsymbol{d}=0$$

and for $\alpha > \alpha_c$,

$$\boldsymbol{x}=[\Theta \quad q]^T, \qquad \boldsymbol{u}=U_T, \qquad \boldsymbol{u}_0=0, \qquad \boldsymbol{d}\neq 0$$

Matrices A and B are system matrices and their values are given in the Appendix. The term $\boldsymbol{d}(\alpha)$ in Eq. (3) is a disturbance component accounting for uncertainties and variations in the model and $\boldsymbol{f}(\alpha, \boldsymbol{x}_0, \boldsymbol{u}_0)$ takes into account the nonzero trim conditions, which may be different at the end of the maneuver. The trim condition values for each phase are also listed in the Appendix.

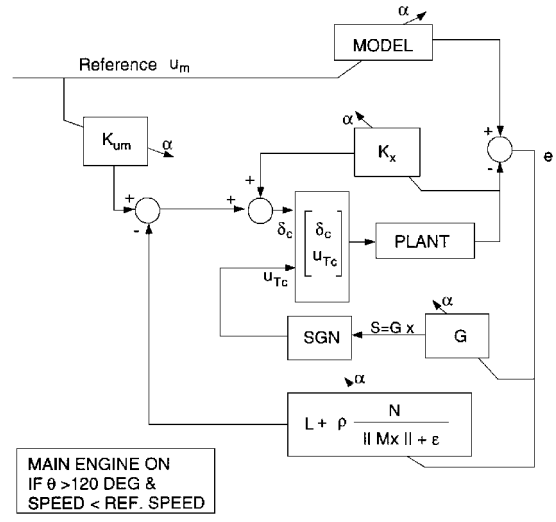

Fig. 2 Autopilot block diagram.

C. Control System Review

The general procedure for the synthesis of the autopilot is based on the theory of variable structure systems.[14–16] The approach has received much attention in the past decade due to its inherent robustness and capability to address the control design of nonlinear systems, with bounded uncertainty. In our application, the variable structure system (VSS) is particularly well suited because the system to be controlled is not only uncertain, but also has reaction jets operating in an on/off fashion, thus allowing a direct implementation of the control law. In the present work autopilot synthesis is carried out based on model following for the entire maneuver and is implemented in the error state space.[6,8,9] The resulting autopilot logic is summarized in Fig. 2.

The model following dynamics are

$$\dot{\boldsymbol{x}}_m(\alpha,t)=A_m(\alpha)\boldsymbol{x}_m(\alpha,t)+B_m(\alpha)\boldsymbol{u}_m(\alpha,t)+\boldsymbol{f}_m(\alpha,\boldsymbol{x}_0,\boldsymbol{u}_0) \tag{4}$$

Equation (4) once again represents the entire maneuver. During the initial and final phases of the maneuver, the state vector models pitch dynamics and flight-path angle. The inputs to the model then are $\boldsymbol{u}_m = [\theta_c \quad \gamma_c]^T$, which are the commanded final pitch attitude and the final flight-path angle commands. During phase II, the system model is a second-order pitch dynamics and in this case the commanded input is $\boldsymbol{u}_m = \theta_c$. A_m and B_m matrices are given in the Appendix.

Variable structure control synthesis is carried out in the error state space, with error dynamics given by

$$\dot{\boldsymbol{e}}(\alpha,t)=A_m(\alpha)\boldsymbol{e}(\alpha,t)+[A_m(\alpha)-A(\alpha)]\boldsymbol{x}(\alpha,t)+A_m(\alpha)\boldsymbol{x}_0+B_m(\alpha)\boldsymbol{u}_m(\alpha,t)-B(\alpha)\boldsymbol{u}-\boldsymbol{d}(\alpha) \tag{5}$$

where $\boldsymbol{e}=\boldsymbol{x}-\boldsymbol{x}_m$. The autopilot is structured as a gain scheduling function of the angle of attack because the error dynamics given in Eq. (5) change according to the α regime. The control law has the general model following form given by

$$\boldsymbol{u}=\boldsymbol{u}_{\mathrm{VSS}}(\alpha)+K_1(\alpha)\boldsymbol{x}(\alpha,t)+K_2(\alpha)\boldsymbol{u}_m(\alpha,t)+K_3(\alpha)\boldsymbol{x}_0(\alpha)+K_4(\alpha) \tag{6}$$

where the expressions of the various terms on the right-hand side (RHS) of the equation change, as mentioned earlier, depending on the phase of the maneuver.

The linear terms appearing in Eq. (6) come directly from the perfect model following condition[9,16] and coincide with the variable structure invariance properties during sliding. The gain matrices are computed as

$$K_1=B^+(A_m-A) \qquad K_2=B^+B_m \qquad K_3=B^+A_m$$
$$K_4=-B^+\boldsymbol{d} \tag{7}$$

where $B^+ = (B^TB)^{-1}B^T$. When the angle of attack is below the critical angle of attack, which is during the initial phase and the final

acquisition of steady state, the gain matrix K_4 is equal to zero ($\boldsymbol{d} = 0$). In the special case when the trim values for attitude and flight-path angles are set to be equal to the model input along with a zero trim pitch rate, the terms $K_3 x_0$ and $K_2 u_m$ cancel out, leaving only the gain matrix K_1 in the low-alpha autopilot structure. During the poststall phase, the only active actuator is the on/off type reaction jet controller, and strictly speaking, the additional linear terms in Eq. (6) are not necessary. Equation (6) for phase II is used in its entirety to verify and show that the equivalent controller remains within the maximum allowable bounds $[-1, +1]$, which guarantees stability. If such a stability condition is satisfied, the control law is then simply given by the nonlinear part; otherwise, the bandwidth of the model in this region must be reduced.

The nonlinear component of the autopilot is the characterizing part of VSS and is a function of the sliding hypersurface $\boldsymbol{s} = G(\alpha)\boldsymbol{e}$. In the low-angle-of-attack region, the expression of $\boldsymbol{u}_{\text{VSS}}$ is chosen to be given by

$$\boldsymbol{u}_{\text{VSS}} = -K_L \boldsymbol{e} - \rho \frac{K_N \boldsymbol{e}}{|K_M \boldsymbol{e}| + \varepsilon} = \boldsymbol{u}^L + \boldsymbol{u}^{\text{NL}} \tag{8a}$$

where the 2×3 gain matrices K_L, K_M, and K_N and the sliding manifold matrix $G(\alpha)$ are computed using an optimal control approach and reduced order error dynamics during sliding.[17] The smoothing parameter ε in Eq. (8a) eliminates chattering of the elevator, whereas the second row on the RHS is replaced by

$$u_T = \text{sgn}[s_2] = \begin{cases} -1 & s_2 > 0 \\ 0 & s_2 = 0 \\ 1 & s_2 < 0 \end{cases} \qquad \text{with} \quad s_2 = [g_{21} \quad g_{22} \quad g_{23}]\boldsymbol{e} \tag{8b}$$

During the high-alpha phase, only reaction jet control is available and the nonlinear component is simply

$$u_T = -\text{sgn}[s] = \begin{cases} -1 & s > 0 \\ 0 & s = 0 \\ 1 & s < 0 \end{cases} \qquad \text{with} \quad s = G\boldsymbol{e} = [g_1 \quad g_2]\boldsymbol{e} \tag{8c}$$

In this case, the error vector has only two components.

The autopilot just described has a feedback structure in error dynamics and operates with the elevator and reaction jets. During the maneuver, however, this is not sufficient to provide compensation for the loss in dynamic pressure and rotation of the flight-path angle direction. To this end, an outer loop consisting of the main engine operating at continuous thrust is introduced. The engine could be operational during the entire maneuver or, if multiple boost capability is available as assumed herein, whenever the attitude angle reaches a preset threshold (120 deg) so that the added acceleration provides flight-path angle rotation and increases the speed to achieve the original reference velocity to complete the heading reversal maneuver.

Performance of the resulting control system are summarized at the end of the next section.

D. Blending

In addition to the control logic, a blending block is introduced between control input and aerodynamic surfaces and reaction jets for the low-angle-of-attack portion of the trajectory (phases I and III).[10,11] This is done typically in autopilot design at the implementation level, due to the presence of multiple effectors and the coupling of the channels. Unless appropriately optimized, control design may lead to unnecessary activity as each controller strives toward achieving the common objective. Optimal control design is used in the derivation of the VSS component, but this requires a trial-and-error approach for selecting appropriate off-diagonal elements for input weighting matrix in the performance index. The approach discussed here provides a structured tool, in a multi-input/multi-output setting, for an optimized synthesis of such a command mixer with none of the mentioned disadvantages. Details on the formal approach can be found in Ref. 10 and are repeated here as they are applied to the original autopilot synthesis.

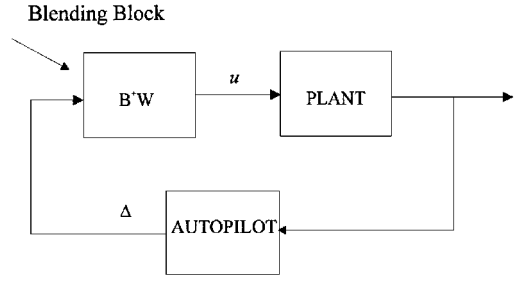

Fig. 3 Autopilot loop schematic with blending.

During the low-angle-of-attack phases of flight, the plant is characterized by two inputs, which are redundant from a pure controllability standpoint. To avoid such difficulties, the original linearized plant given by Eq. (3) is transformed into a single-input equivalent system

$$\begin{aligned} \dot{\boldsymbol{x}}(\alpha, t) &= A(\alpha)\boldsymbol{x}(\alpha, t) + B(\alpha)\boldsymbol{u}(\alpha, t) \\ &= A(\alpha)\boldsymbol{x}(\alpha, t) + W(\alpha)\Delta(\alpha, t) \end{aligned} \tag{9}$$

The new control matrix $W(\alpha)$ lies in the subspace of the original one. The control design is carried out in the equivalent control subspace and then mapped back into the original one generating the appropriate mixing block as shown in Fig. 3.

The determination of the equivalent input term $W(\alpha)\Delta(\alpha, t)$ is performed with the objectives of achieving good performance, with reduced control activity. The methodology used for the computation of elements of the matrix W is based on the application of the Simplex algorithm, once the input Δ is normalized to assumed values equal to either -1 or $+1$ and such that the input identity

$$B(\alpha)\boldsymbol{u}(\alpha, t) = W(\alpha)\Delta(\alpha, t) \tag{10}$$

is satisfied. After some manipulations, necessary to incorporate the sign constraints on the original control vector, a linear programming problem is set up[10] where the index of performance is a linear combination of the elements w_{1i} of column vector $\boldsymbol{W}$ and the constraints are a modified version of Eq. (10):

$$[F_{n\times m} \quad -I_{n\times n} \quad I_{n\times n}] \begin{bmatrix} \boldsymbol{v} \\ \boldsymbol{w}^+ \\ \boldsymbol{w}^- \end{bmatrix} = F_{n\times m}[\mathbf{1}_{m\times 1}], \qquad v \le [2_{m\times 1}] \tag{11}$$

where the vector $\boldsymbol{v} \in [0, 2]$ is the original control vector $\boldsymbol{u}$ normalized to ± 1 deflections. The matrix F is then the scaled input matrix B. The Simplex problem variables are all required to be ≥ 0 and the elements of W are handled by redefining the decision variables w_{i1} in term of w_{i1}^+ and w_{i1}^-. In summary, we need to solve the following problem: Determine the optimal decision vector $\boldsymbol{z} = [\boldsymbol{v} \ \boldsymbol{w}^+ \ \boldsymbol{w}^-]^T \in \mathcal{R}^{m+2n}$ subject to the constraints given by Eq. (11), such that the performance index $J = c_1 w_{11} + \cdots + c_n w_{n1}$ is minimized.

The procedure just outlined is applied to the synthesis of the autopilot in the low-alpha regime. In these phases, the elevator-reaction jet combination is replaced by a single equivalent controller using the identity (10). The new gain matrices obtained by replacing the equivalent controller in Eq. (5) and appearing in Eqs. (6–8) can be found in the Appendix, together with the mixing gain $K_{\text{eq}} = B^+ W$ needed to map the equivalent control into the original one as shown in Fig. 3. Note that the number of gains in the autopilot with blending is reduced by half because the equivalent controller is now a scalar.

The performance of the two autopilots are shown and compared in Figs. 4, 5a, 5b, 6, and 7. Figure 4 shows the elevator deflection and reaction jets activity corresponding to without blending (first column) and with blending (second column) of control. Figures 5a and 5b show the behavior of the missile's angular displacements, while the smooth curve marked with open circles indicates the angular behavior of the model's dynamics. The autopilot with blending (second column of Figs. 4 and 5b) has superior performance in terms of

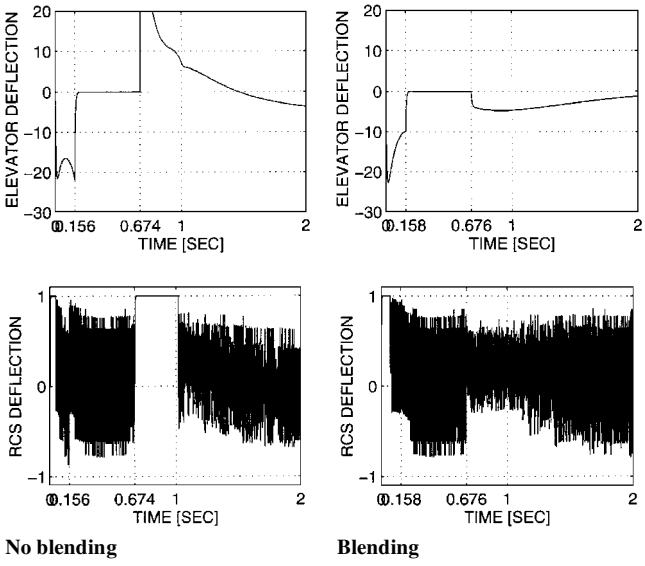

Fig. 4 Control activity without and with blending during heading reversal maneuver.

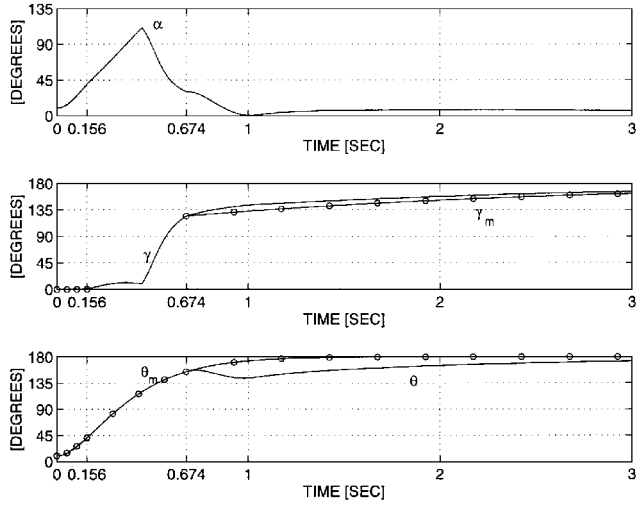

Fig. 5a Angle-of-attack, flight-path, and attitude angles, autopilot without blending.

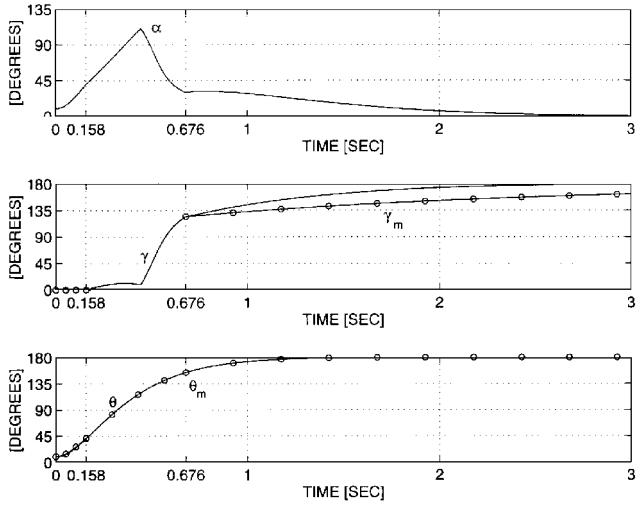

Fig. 5b Angle-of-attack, flight-path, and attitude angles, autopilot with blending.

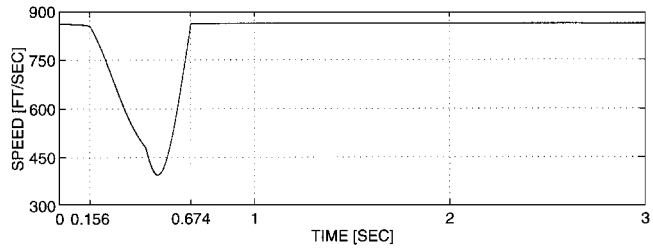

Fig. 6 Velocity variation without and with blending.

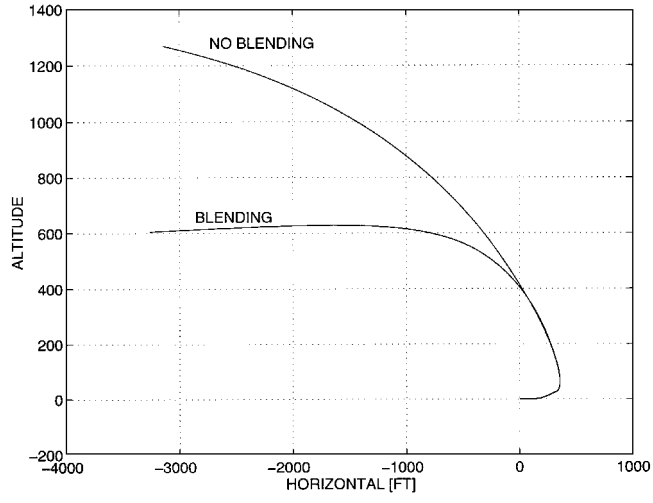

Fig. 7 Maneuver comparison; Mach 0.8.

speed of response and steady-state acquisition and retention. Speed variation between the two control approaches is negligible as seen in Fig. 6. Figure 7 shows that the turn maneuver resulting from blended control is better because the turn radius is considerably reduced.

III. Robustness Analysis

In this section we present an analysis for robustness to parametric variations of the plant described by Eqs. (5) and (6). The relation for stability and robustness is deduced by analyzing Eq. (5) for an off-nominal flight condition by expressing the system matrices as $A = A_N + \Delta A$ and $B = B_N + \Delta B$. The subscript N denotes the nominal case and the prefix Δ is the variation of the matrices with respect to the nominal. We can then rewrite Eq. (5) as

$$\dot{\boldsymbol{e}}(\alpha, t) = A_m(\alpha)\boldsymbol{e}(\alpha, t) + [A_m(\alpha) - A_N(\alpha)]\boldsymbol{x}(\alpha, t) + A_m x_0 + B_m U_m - B_N(\alpha)\boldsymbol{u} - \boldsymbol{d}(\alpha) + \Delta A(\alpha, M)\boldsymbol{x}(\alpha, t) + \Delta B(\alpha, M)\boldsymbol{u}(\alpha, t) \tag{12}$$

Provided that matching conditions on parameter variations are satisfied, substituting the control law given by Eq. (6), and dropping α and t, Eq. (12) simplifies to

$$\dot{\boldsymbol{e}} = A_m\boldsymbol{e} - B_N\boldsymbol{u}_{\mathrm{VSS}} + (\Delta A\boldsymbol{x} + \Delta B\boldsymbol{u}) = (A_m + B_N K_L)\boldsymbol{e} - B_N\boldsymbol{u}^{\mathrm{NL}} + \boldsymbol{h} \tag{13}$$

The function $\boldsymbol{h}$ is a bounded function and it represents, in general, the parametric variations, nonlinearities, and other plant uncertainties. Then the stability and robustness are guaranteed if[18]

$$\boldsymbol{u}^{\mathrm{NL}} \le -\rho\frac{B_2^{-1}[0 \quad P]z}{\|[0 \quad P]z\|}, \qquad z \ge 0, \qquad \rho = \|\boldsymbol{h}\|_2$$
$$\boldsymbol{u}^{\mathrm{NL}} \ge -\rho\frac{B_2^{-1}[0 \quad P]z}{\|[0 \quad P]z\|}, \qquad z \le 0, \qquad \rho = \|\boldsymbol{h}\|_2 \tag{14a}$$

or, in the case of inputs of the on/off type,

$$\boldsymbol{u}_{\min} \le \boldsymbol{u}_{\mathrm{VSS}} \le \boldsymbol{u}_{\max} \tag{14b}$$

Table 1 Geometric and flight condition variations for robustness analysis

Run number	Initial Mach	Final Mach	RJC thrust, lb	Attitude, deg engine on
1	0.8	0.8	500	120
2	0.8	0.8	500	130
3	0.8	0.8	500	140
4	0.6	0.6	500	120
5	0.6	0.6	1000	120
6	0.8	0.8	1000	120
7	1.2	1.2	500	120
8	1.2	1.2	1000	120

In Eqs. (14), following the procedure described in Refs. 11 and 16–18, the vector z is obtained from the state vector e after two suitable coordinate transformations, B_2 is a partition of the input matrix B_N in Eq. (13), and $P > 0$ is the solution of a Lyapunov equation that governs the speed with which the system attains a sliding motion.

To verify these results and to obtain some quantitative measure on the system perturbations, Eq. (13) is further simplified. The control vector u^{NL}, reveals that the linear component of the control law is dominated by the elevator deflection. The nonlinear component is, on the other hand, dominated by reaction jets. Considering dominant terms and using Eqs. (6), (8a), and (13), the error equations can be written as

$$\dot{e} = [A_m - B_{N1}K_{L1}]e - B_{N2}\mathrm{sgn}(Ge) + [\Delta A + \Delta BK_1]x + \Delta B_2\mathrm{sgn}(Ge)$$

which becomes

$$\dot{e} = [A_m - B_{N1}K_{L1}]e - B_2\mathrm{sgn}(Ge) + [\Delta A + \Delta BK_1]x$$

where $B_N = [B_{N1}\ B_{N2}]$, $B = [B_1\ B_2]$, and K_{L1} is the first row of the gain matrix K_L. Using Eqs. (14), the condition for robustness is found to be

$$\|B_2\|_2 \geq \|\Delta A + \Delta BK_1\|_2\|x\|_2 \geq \|[\Delta A + \Delta BK_1]x\|_2 \qquad (15)$$

As compared to Eq. (14), this equation provides us with conservative estimates for the upper limit on the perturbation sizes of the linearized nominal system.

Validation of the autopilot structure, i.e., its stability and robustness, is now shown through several simulation runs of the nonlinear system to various parametric changes listed in Table 1. Run 1 corresponds to the nominal condition. This condition was used to design the two autopilots described in the preceding section, and the corresponding gains were retained for all of the other flight conditions. Both the autopilots presented in the paper (the first one without blending and the second one with blending) were used to compare performance. Complete time histories for the state variables can be found elsewhere in the literature.[19] The model dynamics in Eq. (4) were not changed during the simulation from those relative to the nominal case (run 1). A change in desired model properties could, indeed, lead to further improvement.

Figures 8 and 9 show the trajectories as functions of the Mach number for nominal reaction jet thrust setting and firing of the main engine. Figure 8 is relative to the autopilot without blending. Different trajectories within the same autopilot structure are obtained due to the fact that the same model dynamics are followed, thus resulting in wider turns at higher speed. Although not evident from the figures, due to the short duration of the maneuver, the autopilot with blending allows the completion of the first two phases of flight in a much shorter time. The influence of changing the attitude at which the main engine is fired on the maneuver is shown in Figs. 10 and 11 for nominal speed and reaction jet thrust. Again the autopilot with blending performs much better. As the attitude angle of initial firing increases, the turn is delayed but it has a smaller turn radius. Of course, the analysis for optimal firing time requires a more formal approach to the problem and constitutes a topic of current research

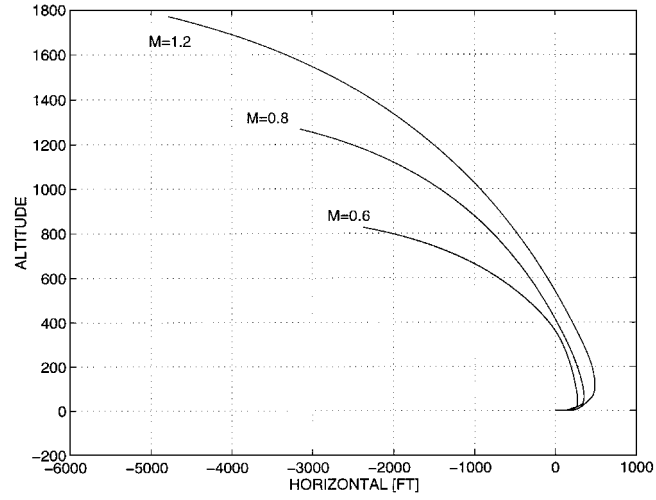

Fig. 8 Maneuver variation with Mach number, no blending.

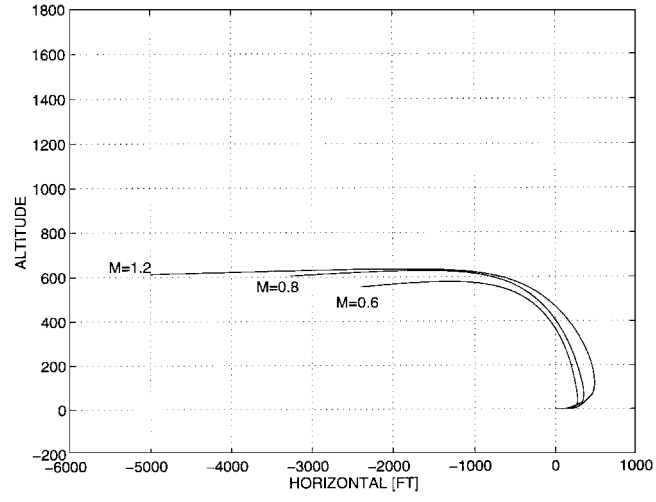

Fig. 9 Maneuver variation with Mach number, with blending.

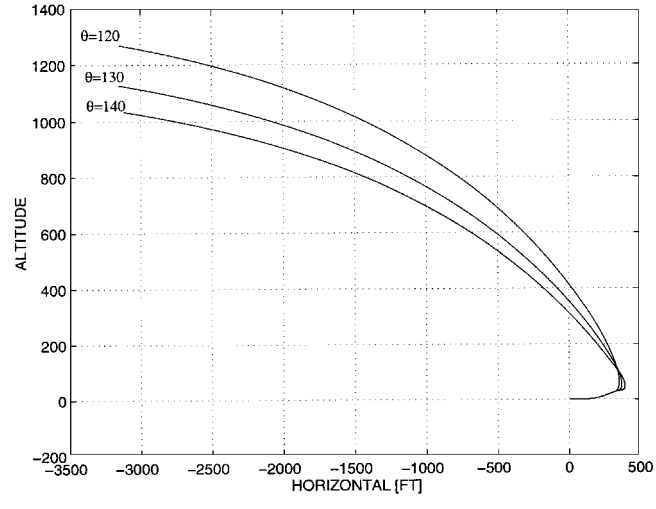

Fig. 10 Maneuver variation with attitude at main engine firing, no blending.

efforts.[20] Performance analysis for different reaction jet thrust values was also performed, and the results shown in Figs. 12 and 13 are for a higher thrust setting.

Another measure of the amount of successfully stabilized perturbations is given by the ratio between the perturbation and nominal matrix norms, relative to Mach number variations. This ratio is shown in Table 2 and gives an indication of the size of parameter variations handled by the controller.

Table 2 Mach number perturbation scale

	Mach variation,%	
Norm ratio	0.8–0.6	0.8–1.2
$\|\Delta A\|/\|A_N\|$	38	9
$\|\Delta B\|/\|B_N\|$	40	9

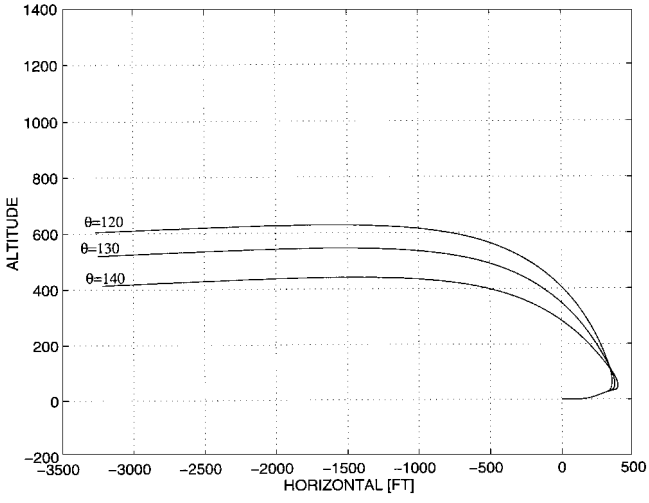

Fig. 11 Maneuver variation with attitude at main engine firing, with blending.

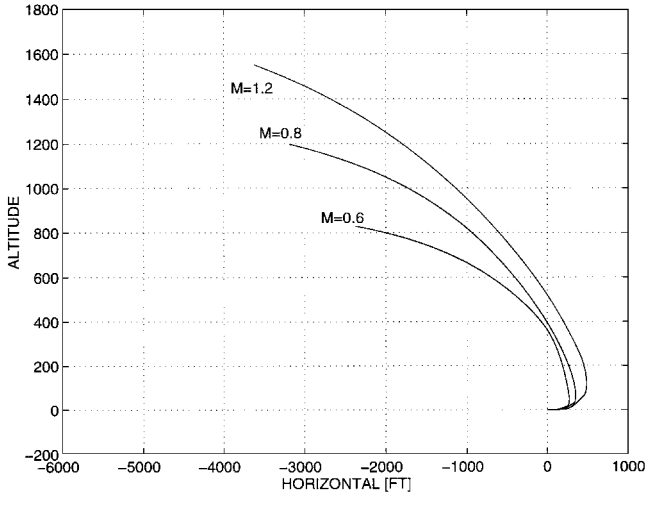

Fig. 12 Maneuver variation with Mach number, no blending, jet thrust = 1000 lb.

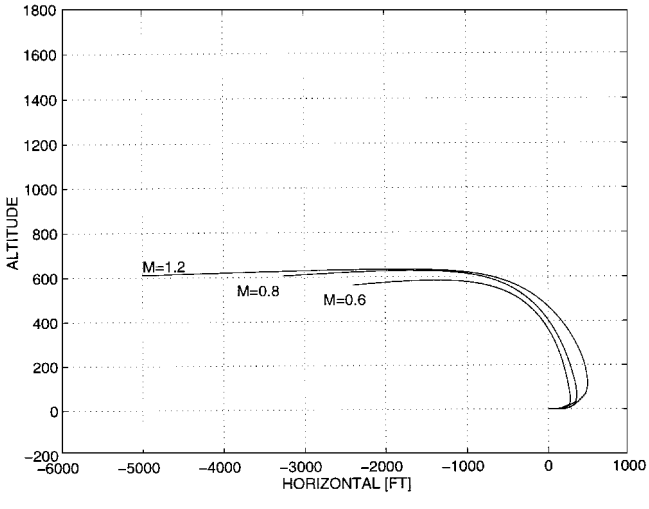

Fig. 13 Maneuver variation with Mach number, with blending, jet thrust = 1000 lb.

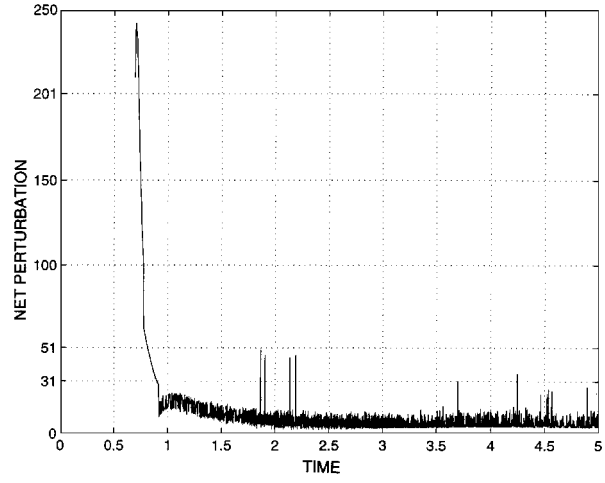

Fig. 14 Validation of condition for robustness for run 7.

The conditions obtained for robustness and stability point out that if parametric variations are bounded and satisfy Eq. (15) then we have robust response. To verify Eq. (15), the RHS of the inequality is obtained by plotting $\|\dot{\boldsymbol{e}} - A_m \boldsymbol{e} + B_N \boldsymbol{u}_{\mathrm{VSS}}\|_2$ with respect to time. For run 7 it is seen (Fig. 14) that once the linear part of the controller drives the system onto the sliding surface, the controller provides a robust response because the perturbation quantity is well within the boundary $\|B_2\|_2 = 31$. Robustness is also satisfied by the other runs (1, 4) provided the norm of $\boldsymbol{x}$ is less than 0.3 and less than 0.6 if the reaction jets thrust is increased to 1000 pounds (runs 5,6, and 8).

IV. Conclusions

A synthesis of a missile pitch autopilot was presented. A model following variable structure approach was used to implement a robust control during a high-angle-of-attack maneuver. Robustness was verified analytically with respect to bounded uncertainties and numerically by performing nonlinear simulation over a range of parameter variations and flight conditions without gain scheduling. The autopilot structure was further improved by introducing a blending gain matrix, which optimizes the relative activity of elevator and reaction jets with respect to the originally proposed controller.

Appendix: System and Gain Matrices

Actuators are modeled as first-order systems (time constant of 1/180 and 1/500 s).

Phases I and III:

$$A = \begin{bmatrix} 0 & 1 & 0 \\ -33.4266 & 0 & 33.4266 \\ 0.1647 & 0 & -0.1647 \end{bmatrix} \qquad B = \begin{bmatrix} 0 & 0 \\ -90.5355 & 31.0490 \\ 0.1836 & 0.0829 \end{bmatrix}$$

$$A_m = \begin{bmatrix} 0 & 1 & 0 \\ -25 & -10 & 0 \\ 0 & 0 & -0.5 \end{bmatrix} \qquad B_m = \begin{bmatrix} 0 & 0 \\ 25 & 0 \\ 0 & 0.5 \end{bmatrix}$$

Phase II:

$$A = \begin{bmatrix} 0 & 1 \\ 0 & 0 \end{bmatrix} \qquad B = \begin{bmatrix} 0 \\ 31.049 \end{bmatrix} \qquad \boldsymbol{d} = \begin{bmatrix} 0 \\ -10 \end{bmatrix}$$

$$A_m = \begin{bmatrix} 0 & 1 \\ -25 & -10 \end{bmatrix} \qquad B_m = \begin{bmatrix} 0 \\ 25 \end{bmatrix}$$

Trim $(\boldsymbol{x}_E, \boldsymbol{u}_E)$ and initial conditions $(\boldsymbol{x}_0, \boldsymbol{u}_0)$, with angles in degrees, for phase I

$$\boldsymbol{x}_E = \begin{bmatrix} 10 \\ 0 \\ 0 \end{bmatrix} = \boldsymbol{x}_0, \qquad \boldsymbol{u}_E = \boldsymbol{u}_0 = 0$$

for phase II

$$\boldsymbol{x}_0 = \boldsymbol{x}(\alpha = 40^+), \qquad \boldsymbol{u}_0 = \boldsymbol{u}(\alpha = 40^+)$$

and for phase III

$$\boldsymbol{x}_E = \begin{bmatrix} 180 \\ 0 \\ 180 \end{bmatrix}, \qquad \boldsymbol{u}_E = 0 \qquad \text{and} \qquad \boldsymbol{x}_0 = \boldsymbol{x}(\alpha = 40^-)$$

$$\boldsymbol{u}_0 = \boldsymbol{u}(\alpha = 40^-)$$

Autopilot gains without blending for phases I and III

$$K_1 = \begin{bmatrix} -0.4402 & 0.0628 & -0.5785 \\ -1.0121 & -0.1391 & -2.7635 \end{bmatrix}$$

$$K_2 = \begin{bmatrix} 0.1569 & 0.0628 & -1.1756 \\ -0.3476 & -0.1391 & -3.4279 \end{bmatrix}$$

$$K_3 = \begin{bmatrix} -0.1569 & 1.1756 \\ 0.3476 & 3.4279 \end{bmatrix}$$

$$K_L = \begin{bmatrix} -0.1073 & 0.01184 & -2.3513 \\ -0.3329 & -0.10836 & -6.8558 \end{bmatrix}$$

$$K_M = \begin{bmatrix} 0.00048 & 0.00068 & 0.33333 \\ -0.05051 & -0.07143 & 0.00015 \end{bmatrix}$$

$$K_N = \begin{bmatrix} -0.00057 & -0.00080 & -0.78372 \\ -0.00328 & -0.00464 & -2.2853 \end{bmatrix}$$

and for phase II

$$K_1 = [-0.8052 \quad -0.3221]$$

$$K_2 = [1.5781 \quad 0.80518], \qquad K_4 = -0.3221$$

Autopilot gains with blending (phases I and III only)

$$K_1 = [0.1345 \quad -0.1596 \quad -0.5336] \qquad K_2 = [0.333 \quad 0]$$

$$K_3 = [-0.399 \quad -0.1596 \quad 0]$$

$$K_L = [0.3200 \quad 0.0366 \quad 0] \qquad K_M = [-0.0505 \quad -0.0714 \quad 0]$$

$$K_N = [-0.0008 \quad -0.0011 \quad 0]$$

The cost functional minimized by the Simplex algorithm was given by

$$z = \sum_{i=1}^{3} w_i$$

leading to

$$W = [0 \quad 62.6497 \quad 0.0188]^T \qquad \text{and} \qquad K_{\text{eq}} = [-0.349 \quad 1]^T$$

Acknowledgments

The work of the first author was partially supported by the U.S. Air Force Material Command, Wright Laboratory, under Grant F08630-94-1-0001. Frederick A. Davis, WL/MNAV (Flight Vehicles Branch, Wright Laboratory), served as Technical Monitor.

References

[1]Anon., "Operational Agility," AGARD-AR-314, Flight Mechanics Panel, NATO, April 1994.

[2]Cliff, E. M., Lutze, F. H., Thompson, B. G., and Well, K., "Toward a Theory of Aircraft Agility," AIAA Paper 90-2808, Aug. 1990.

[3]Lawless, A., "Aircraft Agility Measurement Research and Development," AFFTC-TIM-91-01, June 1991.

[4]Wulff, G., and Zoellner, M., "DIVA/MIMO Flight Test Data Analysis for the X31-A Demonstrator," AIAA Paper 91-2852, Aug. 1991.

[5]Bowers, A. H., Regenie, V. A., and Flick, B. C., "F-18 High Alpha Research Vehicle: Lesson Learned," Fourth High Alpha Conf., NASA-DFRC, July 1994.

[6]Innocenti, M., and Thukral, A., "Simultaneous Reaction Jet and Aerodynamic Control of Missile Systems," AIAA Paper 93-3739, Aug. 1993.

[7]Anon., "Special Course on Missile Aerodynamics," AGARD-R-804, Fluid Dynamics Panel, NATO, June 1994.

[8]Innocenti, M., Thukral, A., and Cochran, J. E., Jr., "Evaluation of Variable Structure Control for Missile Autopilot Using Reaction Jets and Aerodynamic Control," Dept. of Aerospace Engineering, Final Rept., Grant RDL-93-132, Auburn Univ., Auburn, AL, Feb. 1994.

[9]Thukral, A., and Innocenti, M., "Missile Pitch Autopilot for High Angle of Attack Maneuvering," *IEEE Transactions on Control Systems Technology* (submitted for publication).

[10]Innocenti, M., and Thukral, A., "A Blending Strategy for Missile Autopilots Using the Simplex Method," *Proceedings of the American Control Conference*, Seattle, WA, June 1995.

[11]Thukral, A., "Design of Missile Flight Control Systems Using Variable Structure Techniques," Ph.D. Dissertation, Dept. of Aerospace Engineering, Auburn Univ., Auburn, AL, May 1995.

[12]Bruns, K. D., et al., "Missile DATCOM, Users Manual - Rev 4/91," Final Rept., WL-TR-91-3039, May 1987–April 1991.

[13]Hoerner, S., *Practical Information on Fluid Dynamic Drag*, Wiley, New York, 1958.

[14]Utkin, V. I., *Sliding Modes and Their Application in Variable Structure Systems*, MIR, Moscow, 1978, pp. 43–55.

[15]Itkis, U., *Control Systems of Variable Structure*, Wiley, New York, 1976.

[16]Zinober, A. S. I., "Deterministic Control of Uncertain Systems," IEE-40, Control Engineering Series, 1990.

[17]Thukral, A., and Innocenti, M., "Controls Design Challenge: A Variable Structure Approach," *Journal of Guidance, Control, and Dynamics*, Vol. 17, No. 5, 1994, pp. 942–969.

[18]Ryan, E. P., and Corless, M., "Ultimate Boundedness and Asymptotic Stability of a Class of Uncertain Dynamical Systems via Continuous and Discontinuous Feedback Control," *IMA Journal*, Vol. 1, 1984, pp. 223–242.

[19]Thukral, A., and Innocenti, M., "Uses of VSS for Autopilot Design of Nonlinear Flight Vehicles," Third Workshop on Robust Control via Variable Structure and Lyapunov Techniques, Benevento, Italy, Sept. 1994.

[20]Innocenti, M., "Integrated Approach to Guidance and Control of Alternate Control Technology Flight Vehicles," Annual Rept., Grant AMFC-F08630-94-1-0001, Univ. of Pisa, Italy, Nov. 1995.